East European Journal of Physics. **2.** 219-231 (2026)
DOI:10.26565/2312-4334-2026-2-23 ISSN 2312-4334

COMPARATIVE EFFECTS OF COLD PLASMA AND THERMAL ANNEALING ON THE STRUCTURAL AND MORPHOLOGICAL PROPERTIES OF NICKEL AND IRON OXIDE COATINGS

Aya Jumaa, Duha K. Harfesh, A.N. Yasoob*, Hamid H. Murbat
University of Baghdad, College of Science for Women, Department of Physics, Baghdad, Iraq
**Corresponding Author email: Noorya_phys@csw.uobaghdad.edu.iq*
Received January 25, 2026; accepted April 30, 2026

This study comprehensively investigates and compares the effects of Cold Atmospheric Plasma (CAP) treatment as a potential alternative to thermal annealing on the structural and morphological properties of two distinct thin films: nickel (Ni) and iron oxide (Fe_xO_γ), both electrochemically deposited on ITO substrates. Characterization via X-ray diffraction (XRD) and atomic force microscopy (AFM) revealed that the material's nature dictates its response to post-processing. For nickel, short-duration CAP exposure (2.5-5 min) optimally enhanced crystallinity and surface smoothness by reducing grain size and roughness, while longer exposures led to oxidation and increased roughness. Conversely, for iron oxide, even brief CAP treatment initiated a transformation from monocrystalline to polycrystalline structure, forming a mixture of phases (Fe_3O_4, γ-Fe_2O_3). The smoothest iron oxide surface was achieved after 5-10 minutes of CAP, with excessive exposure (15 min) causing surface damage. Thermal annealing proved superior for nickel at 200°C, yielding the smallest grains and smoothest surface. However, it was inadequate for optimal iron oxide crystallization. This work demonstrates that CAP as a fast, energy-efficient alternative to conventional annealing. The optimal parameters are highly dependent on the material-specific and crucial for tailoring functional coatings in catalysis and sensing.
Keywords: *Cold Plasma; DBD; Plasma annealing; Nickel coating; Iron oxide; Hematite; Magnetite*
PACS: 52.77.-j, 81.15.Pq, 68.55.-a, 61.05.cp, 68.37.Ps, 52.50.Jm, 61.66.Fn, 81.40.Ef, 81.40.Rs

1 INTRODUCTION

Non-thermal plasma is one of the technologies that has wide applications in industry and medicine, such as oxidation [1], affection on living tissue [2], and synthesis nanoparticles [3]. Furthermore, the high energy of plasma is capable of annealing materials through surface treatment. Annealing is a critical process used to enhance the properties of various materials through controlled heating and cooling [4, 5]**.** Annealing can lead to a reduction in grain size, improve crystallinity, hardness, and electrical conductivity [6]. Many annealing techniques have been improved. The thermal annealing technique is a common method [7] involves heating a material to a specific temperature, maintaining that temperature for a set duration, and then cooling it [8]. Another method that can be used for annealing is treating with plasma [9,10]. The physical and chemical properties of materials may be modified by exposure to cold plasma. This improve wettability in polymers, raising surface energy and altered chemical compositions [11]. Plasma exposure affects recrystallization behavior by slowing down recrystallization, thus preserving mechanical strength, enhancing activation of metal surfaces, and altering surface morphology [12]. There are many types of plasma production systems that are used in annealing material, such as hollow cathode discharge, RF plasma annealing[13], atmospheric pressure plasma jet [14]. One of these systems is the dielectric barrier discharge [15], (DBD plasma) can be used in surface annealing [16, 17]; DBD plasma systems typically consist of two electrodes, with at least one covered by a dielectric material. This setup prevents the formation of a continuous arc and allows for the generation of microdischarges. The dielectric barrier causes the formation of numerous microdischarges, which are small, transient plasma channels that occur between the electrodes. These microdischarges are responsible for the generation of reactive species [18]. These species are effective in breaking down pollutants and sterilizing surfaces [19]. The electrical model of DBD plasma includes components like stray inductance and air-gap capacitance, which create voltage and current oscillations. These oscillations are damped by plasma resistance, ensuring a stable and streamer-free plasma discharge. It can operate at atmospheric pressure without the need of vacuumed system [20] and the low-temperature nature of DBD plasma prevents thermal damage to heat-sensitive materials [21]. The mechanisms underlying DBD plasma annealing involve interactions between reactive plasma species (e.g., ions, radicals, and UV photons) and the material surface. These interactions of reactive species lead to new functional groups (e.g., –COH, –COOH) on the surface, enhancing chemical activity and wettability [22].Plasma treatment can increase surface roughness, improving mechanical interlocking and adhesion properties [23].

In this work, we compared the conventional technique of annealing based on heating with annealing by DBD plasma for iron oxide and nickel thin films prepared by electrochemical deposition, and studied their structural characteristics using X-ray diffraction (XRD) to investigate the crystallinity and phase changes and atomic force microscopy (AFM) to measure the changes in surface roughness.

Cite as: A. Jumaa, D.K. Harfesh, A.N. Yasoob, H.H. Murbat, East Eur. J. Phys. 2, 219 (2026), https://doi.org/10.26565/2312-4334-2026-2-23

2. MATERIALS AND METHODS

A nickel electrolyte solution was prepared by dissolving 1.5 M of Nickel (II) sulfate hexahydrate $NiSO_4$ $(H_2O)_6$, 0.3 M of Nickel (II) chloride ($NiCl_2$) and 0.7 M of boric acid (H_3BO_3) are added to 25 ml of de-ionized water. The solution was heated 75℃ whiles being stirred with a magnetic stirrer until it had completely dissolved. The pH of the resulting solution was measured and found to be 4.5.

To prepare iron aqueous electrolytes, 0.5 M ferrous chloride (FeCl2) and 0.4 M boric acid (H3BO3) was made by dissolving in 100 ml of deionized water at 25℃.The solution was stirred on a magnetic stirrer until all components were fully dissolved, and the final pH was adjusted to 3.

A simple solution-based method, electrochemical deposition depends on oxidation-reduction reactions within an electrochemical cell. This cell consists of two electrodes, cathode as the working electrode and the anode as counter electrode. The chemical reaction occurring at the electrode surface depends on potential difference across these two electrodes that is controls by the transformation of electrons that drives the chemical reactions at the electrode surfaces.

The cell operated by DC power supply, and the voltage and current flowing between the electrodes control the chemical processes.

For deposition of nickel, the anode is made of pure nickel (99.9%), and in the case of deposition of iron, the anode is made of stainless steel. The cathode is a substrate made of indium tin oxide(ITO) on which the electrolyte is deposited. The nickel electrolyte, prepared in a laboratory and maintained at 75℃, is placed on the heater to keep its temperature at 75℃ for deposition on the cathode. Both electrodes are immersed in the electrolyte-filled flask, with a small distance between them of less than 1 cm. The chemical interaction that achieved efficient deposition began at a voltage (4.5 V) and current (0.5 A) for 10 seconds of the deposition process.

During iron oxide deposition, the stainless-steel electrode is reached to the positive terminal of power supply and make it anode, and the (ITO) substrate reached to negative terminal of power supply serving as a cathode. Both electrodes are immersed in the electrolyte solution at room temperature. The chemical interaction that achieved efficient deposition began at a voltage (10 V) and current (0.5 A) for 5 seconds, the electrolyte deposited homogenously.

The prepared thin films of nickel and iron were exposed to a cold plasma discharge device, which included a high-voltage power supply (AC) and two electrodes made of stainless steel. the magnitude of applied voltage about (15 kV) A glass dielectric medium was used to protect the electrical contact between the electrodes and was positioned between them to maintain plasma discharge stability and safety. The prepared films were exposed to the plasma for (2.5, 5, 10 and 15) minutes.

The prepared thin films have been treated by the conventional method of annealing using heat in a furnace at 200°C and 400°C for two hours, and compared with the results of annealing by DBD. The samples were prepared and processed to examine improvements in their structural and crystalline properties using “XRD, and AFM” for all samples, control, after exposure to cold plasma, and annealed samples by high temperature annealing.

RESULTS AND DISCUSSION

X-ray Diffraction Results

The XRD patterns of the prepared nickel and iron oxide synthesized via electrochemical deposition were measured using X-ray diffraction instrument from the Netherlands by Philips Company (PW1730).

X-ray diffraction of nickel

Fig. 1 represents the XRD pattern of electrochemically deposited nickel before annealing or exposing to cold plasma (control)The figure clarifies peaks belong to nickel oxide (Ni_2O_3) at $2\theta = 30.392^o$ correspond to (002) plane, 44.542^o and 52.553^o belong to (FCC) nickel element (Ni) correspond to (111) and (200) miller indices respectively according to The other two peaks of refer to hexagonal structure of Ni $(OH)_2$ at $2\theta = 19.581^o$ and 33.408^o the orientations are:(001) and (100) respectively. These results have been matched with JCPDS files no. (00-014-0481), (00-003-1043) and (00-003-0177) [24].

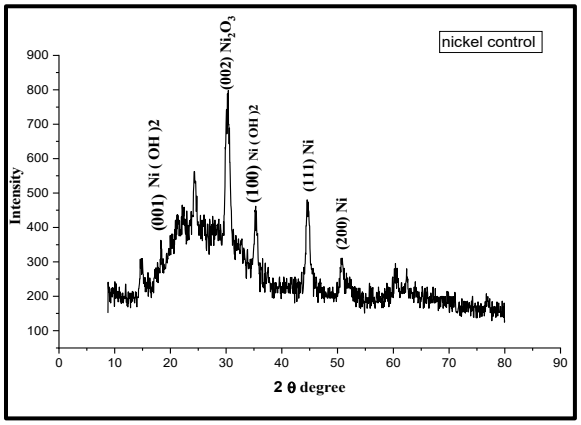

Figure 1. XRD diffraction of nickel prepared by electro chemical deposition before annealing by heating or exposing to plasma.

Furthermore, we used the Scherrer equation [25] to determine the crystalline size of nickel by analysis of the peak broadening by using Eq. 1:

$$D = \frac{k\,\lambda}{\beta \cos\theta} \tag{1}$$

It was found the average crystalline size is about 11 nm. Fig (2) represented the XRD pattern for samples after exposed to cold plasma, from Fig. (2a) we noted that after exposed the sample to cold plasma for 2.5 min, an increased in the intensity of the nickel peaks at angles 44.5° and 52°, indicating an increase in its crystallinity.

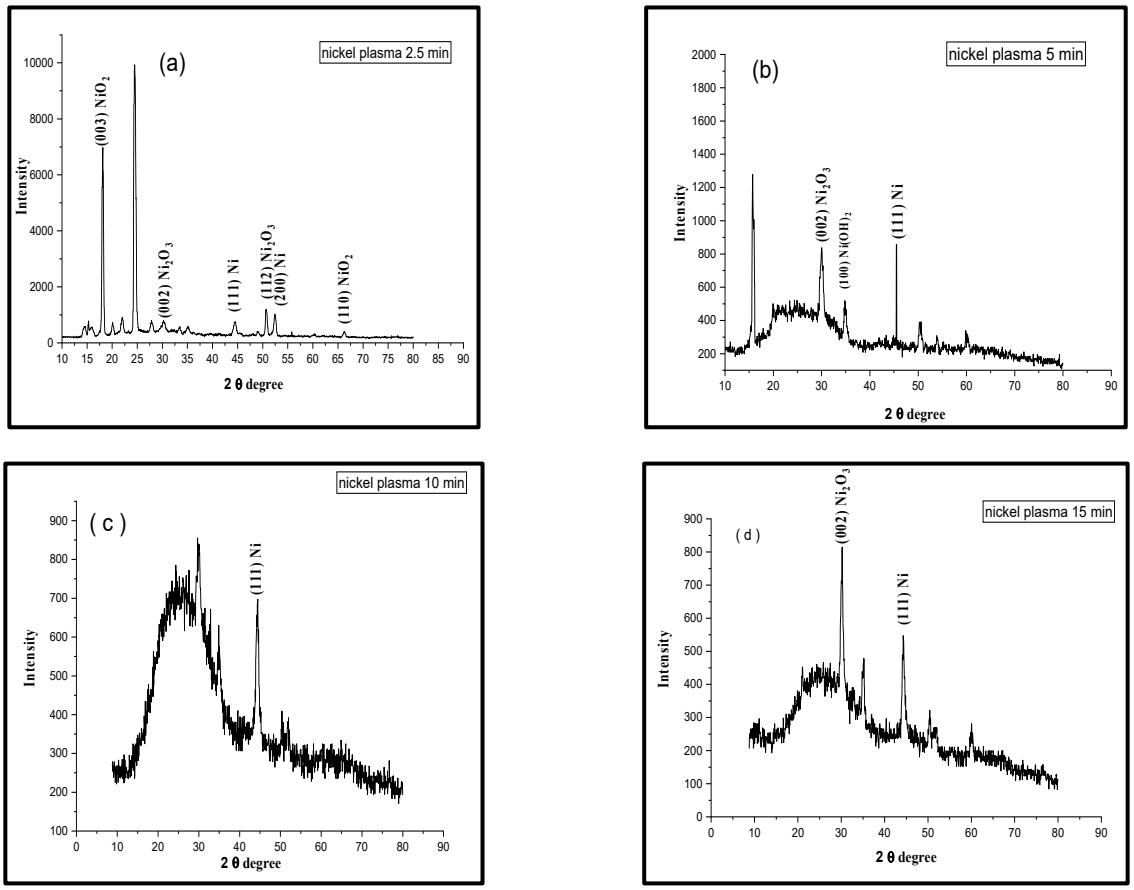

Figure 2. XRD of nickel after exposing to plasma for: (a): 2.5 min, (b): 5 min, (c):10 min, (d): 15 min

This was accompanied by the growth of other peaks, suggesting the emergence of other phases as well as nickel oxides. Additionally, a decrease in the background was observed, indicating good crystallization of the material. The reactive species generated in DBD plasma can be broadly categorized into reactive nitrogen species (RNS) like nitric oxide and nitrogen dioxide [26] and reactive oxygen species (ROS) such as singlet oxygen, atomic oxygen, ozone, and ion The plasma oxidation by ROS may be the main cause of formation of nickel oxide. These ROS rapidly react with nickel surfaces, causing oxidation and formation of nickel oxide layer, also plasma containing a high fraction of dissociated oxygen can form nickel oxide films in seconds, indicating the strong oxidative power of plasma-generated ROS. High dissociation of oxygen in plasma increases the availability of ROS, accelerating the oxidation processes [27].

Furthermore, enhancing the interaction between nickel and its support, leading to improved crystallinity and stability by promoting the formation of nanoparticles with a flat morphology [28]. And lead to formation new phases of nickel oxide in different orientation at 2θ: (18.55°,30.24°,44.59°, 52.230° and 66.192°) corresponding to hkl ((003), (002), (111), (200) and (110)) respectively.

Upon increasing the plasma exposure time starting from 5 minutes, the sample exhibited an increase in the intensity of the Ni (111) peak but less than at (2.5 min), particularly upon reaching 10 minutes of exposure. This was an increase in the intensity of nickel oxide peaks, caused by plasma-induced surface oxidation and the formation of new functional groups. The increased intensity of the nickel oxide peaks indicates enhanced surface oxidation at longer exposure times, resulting from the generation of free radicals and a gradual transformation from metallic nickel to nickel oxides (such as NiO or $Ni(OH)_2$). These oxides are chemically active materials widely used in catalysis, batteries, and sensors, as the process introduced new functional groups suitable for catalytic applications[29, 30]. As observed in Fig. (2d), the sample after 15 minutes of exposure became nearly identical and closely matching the control sample, despite the variations observed at intermediate exposure times (2.5-10 minutes). This suggests surface saturation and reaching to an equilibrium

state, where some oxides decompose, crystal rearrangement occurs, and the crystalline structure returns to one closely resembling pristine nickel. It is noteworthy that this finding aligns with our previous study [15], where chemical changes in the liquid phase were observed to reach saturation after 15 minutes. Prolonged plasma exposure introduces energetic ions and reactive species that can etch the film surface, create defects, and break down crystalline domains, leading to increased amorphization and reduced crystallinity, so short plasma exposures may initially enhance crystallinity by promoting surface mobility and ordering, but exceeding a critical exposure time reverses this effect, transforming the film into an amorphous state [31].

Fig. (3) represented annealed samples for (200, 400)ºC. According to JCPDS files these peaks refer to Ni, NiO_2, Ni_2O_3.This result was compared with nickel film synthesized by the same method. The other peaks that appeared but didn't distinguish as one of the nickel compounds may refer to the rest of precursors or impurities.

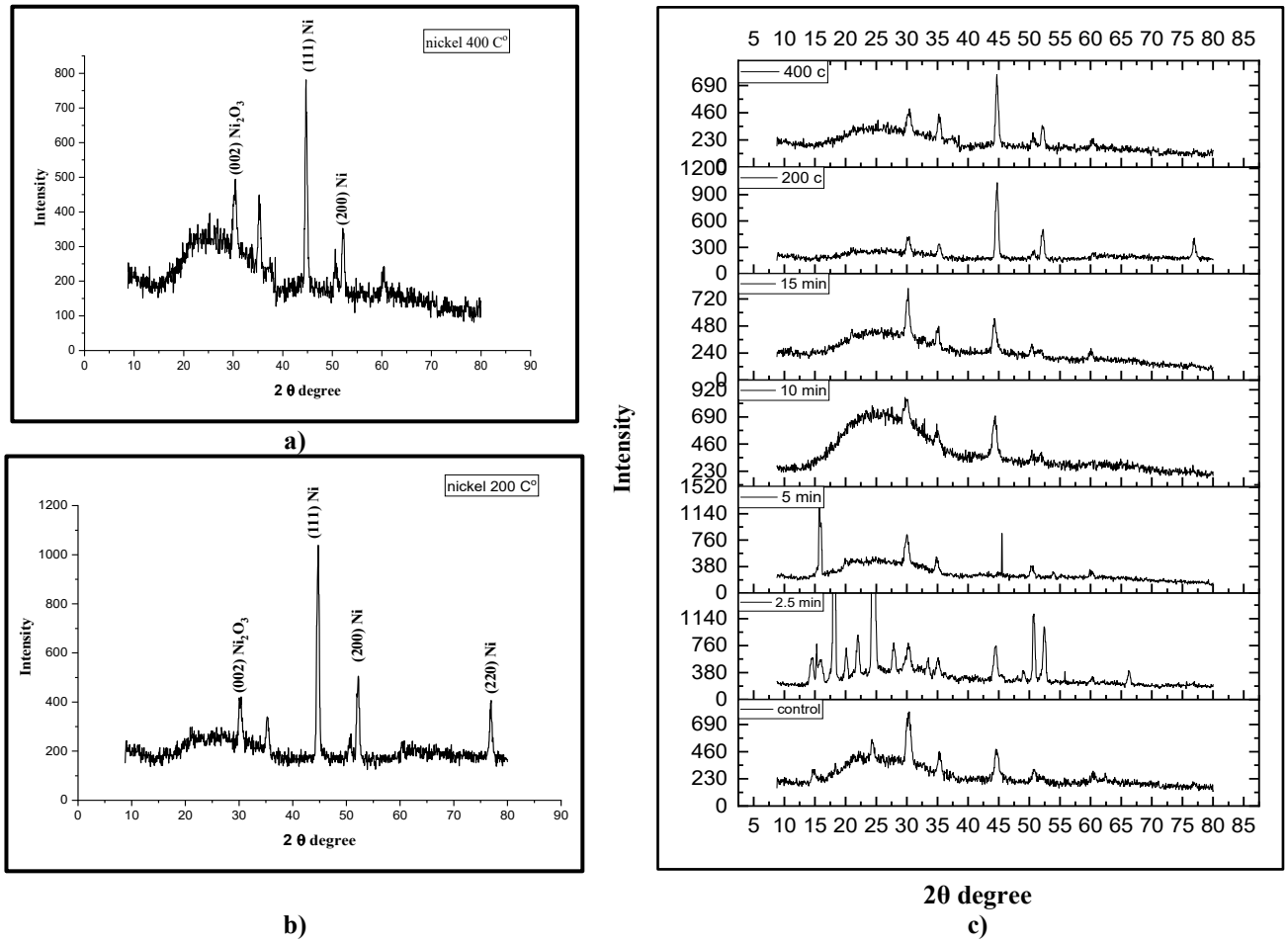

Figure 3. XRD of nickel after heating for: (a) 200°C, (b) 400°C, (c) all treatments (control, (2.5, 5, 10, 15) min, (200, 400)°C

The annealing process is important for enhancing the crystalline structure and functional properties of thin films. It was observed that annealing significantly improves the structure specially at 200°C. This enhancement was evidenced by an increase in crystallite size and the intensity of the Ni (111) diffraction peak. However, when the temperature was raised to 400°C, the crystallinity decreased, as indicated by a reduction in peak intensity. However, conventional thermal annealing typically requires prolonged heating (≈2 hours at 200 °C followed by gradual cooling that may take up to 24 hours), which consumes significant time and energy. In this context, cold plasma has emerged as a relatively fast, low-temperature alternative capable of inducing atomic rearrangement and surface modification within just a few minutes. It is anticipated that this work will contribute to the development of a time- and energy-efficient annealing strategy while preserving the quality of the crystalline structure. Ni as a predominant phase with fine structure. Heating to 400 °C also led to crystalline Ni at nearly the same diffraction angles with less intensity.

Atomic Force Microscopy (AFM) Analysis of Nickel

The surface modification characteristics including morphology and roughness have been tested by atomic force microscopy (Mountains SPIP® Expert8.2.10392). (Fig. 4) illustrates the topographical graphs of nickel thin film (a) control, that subsequently subjected to either to cold plasma treatment for various exposure times (b): 2.5 min, (c): 5 min, (d):10 min, (e): 15 min), and to thermal annealing ((f) 200 °C, (g) 400°C). The surface analysis as summarized in Table (1) evaluated in terms of mean grain size, surface roughness, root mean square, and threshold.

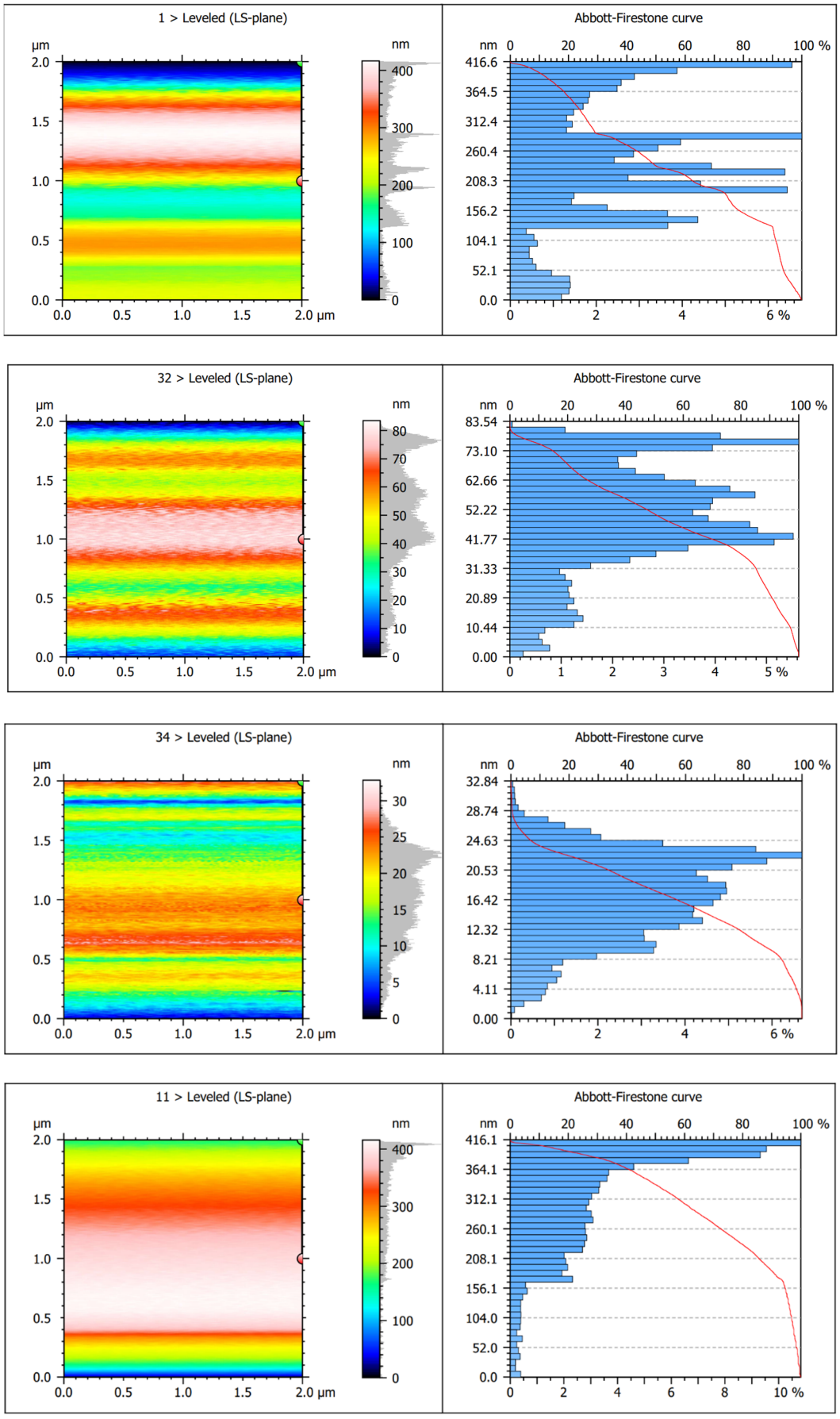

Figure 4. AFM of nickel thin film for: (a) control (b): 2.5 min, (c): 5 min, (d):10 min, (e): 15 min (f) 200 °C, (g) 400 °C

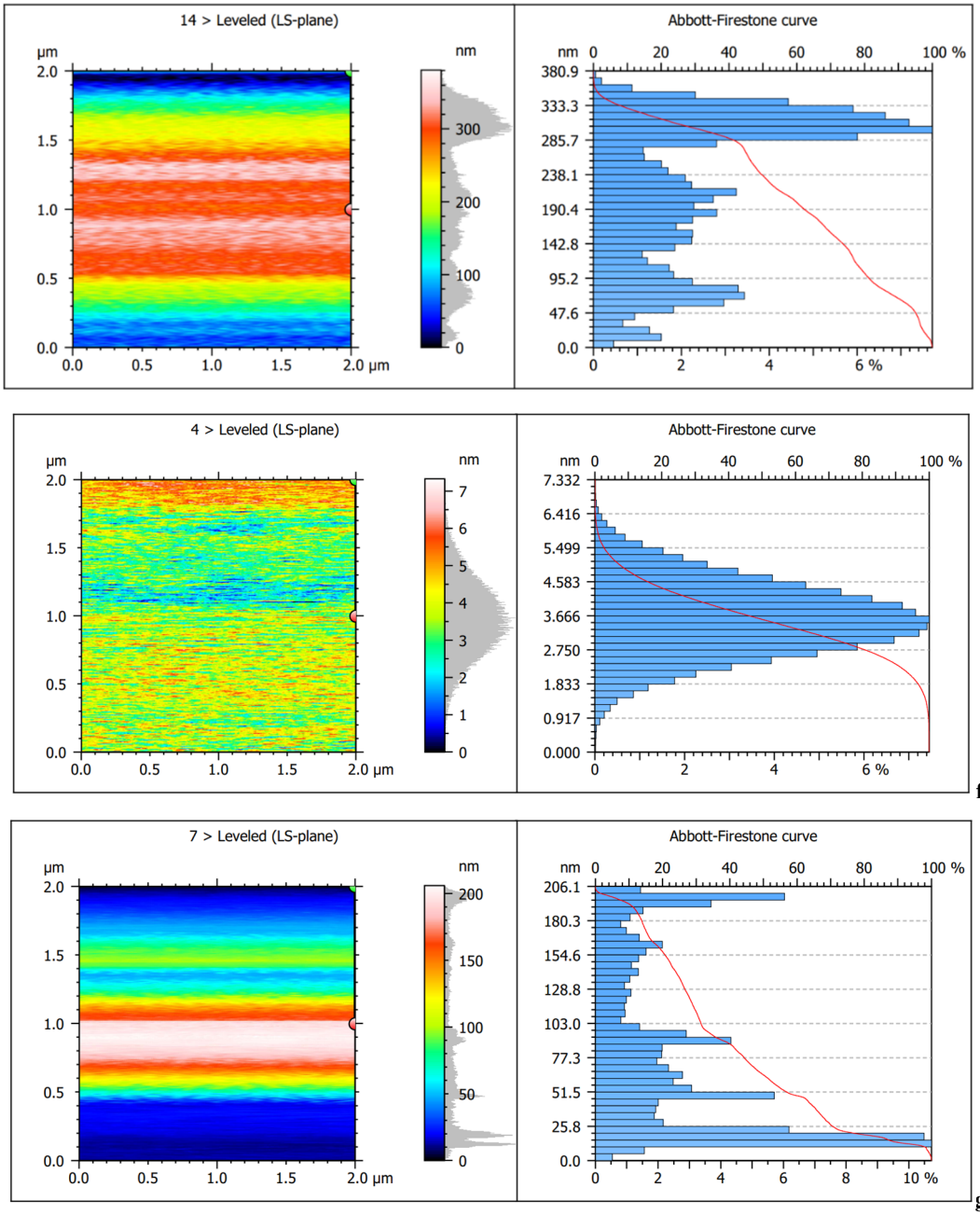

e)

f)

g)

Figure 4. AFM of nickel thin film for: (a) control (b): 2.5 min, (c): 5 min, (d):10 min, (e): 15 min (f) 200 ºC, (g) 400 ºC (*continued*)

(We show that from Fig. (4) the change in grain size, RMS, and roughness between control (Fig. 4a), which has a large grain size (≈ 262 nm) with high roughness and RMS (Ra ≈ 71.6 nm, RMS ≈ 87.2 nm) as listed in Table (1). These values are consistent with a surface that has large grains and pronounced topographical features. Accordingly, the threshold value is also high (≈ 244 nm), reflecting a broad distribution of surface elevations.

Table 1. Summarized the AFM analysis of nickel samples

Samples	mean diameter (nm)	Surface Roughness (nm)	Root Mean Square (nm)	Threshold (nm)
control	262.4	71.60	87.16	243.8
2.5 min	52.77	12.26	14.40	50.12
5 min	17.96	4.572	3.666	17.09
10 min	323.6	41.65	57.42	312.7
15 min	228.2	47.02	57.17	218.7
200 ºC	4.014	0.7064	0.8828	3.594
400 ºC	96.05	39.84	34.09	82.39

After exposure to cold plasma we show that the short intervals (2.5, 5 min) gave better results, the grain size decreases (down to ≈18 nm at 5 min), and reduction in roughness (Ra≈4.6 nm, RMS≈3.7 nm), this is due to the interaction between the components of cold plasma (ions, free radicals ROS and RNS, UV photons) with surface, these species in plasma DBD environment that provides high-energy ions bombard the surface increasing their mobility. This enhanced mobility allows atoms to migrate and fill in surface valleys, leading to a smoother surface by enhancing fusion process. For nickel, the plasma can modify the oxidation states and surface chemistry, potentially leading to a more stable surface layer. This chemical modification can also enhance the adhesion of subsequent layers, contributing to a smoother overall surface [32]. Through these interactions, aggregates with weak bonding removed, and activation of nucleation new sites.This leads to the formation of finer grains and smoother surfaces. The Threshold values decrease correspondingly (≈17–50 nm) as the range of height variations narrows. However, at longer exposure time (10, 15 min) grain size increases again (up to ≈324 nm at 10 min), and roughness rises (Ra≈41–47 nm) and extends to control sample at (15 min) because the continuity of exposure of (CAP), led to the formation of nickel oxide (NiO) on the surface when treated with oxygen plasma. This oxide layer has a smaller domain size compared to the metallic nickel, contributing to the roughness[33]. as well as observed, that in XRD examination as shown in Fig. 2d. As a result of annealing that shown in (Fig. 4f) & (Fig. 4g), at 200℃ gave smallest grain size and (≈4 nm) with extremely low roughness (Ra≈0.71 nm, RMS≈0.88 nm) and a very low Threshold (≈3.6 nm), which led to smooth surface. At an annealing temperature 400℃, grain size and roughness decrease, though they do not achieved at 200℃. At this temperature, bulk diffusion is activated, leading to grain growth and stronger grain boundary definition.

X-ray diffraction of iron oxide

X-ray diffraction was used to study the electrochemical deposition of (FeCl2) solution on an ITO substrate. The XRD patterns prior to heating and plasma exposure are presented in Fig. 5. A single intense peak is observed at 2θ = 44.34°, which corresponds to the (400) orientation of magnetite (Fe_3O_4) according to JCPDs file no.: (1317-61-9), This indicates that the method successfully synthesized monocrystalline iron oxide.

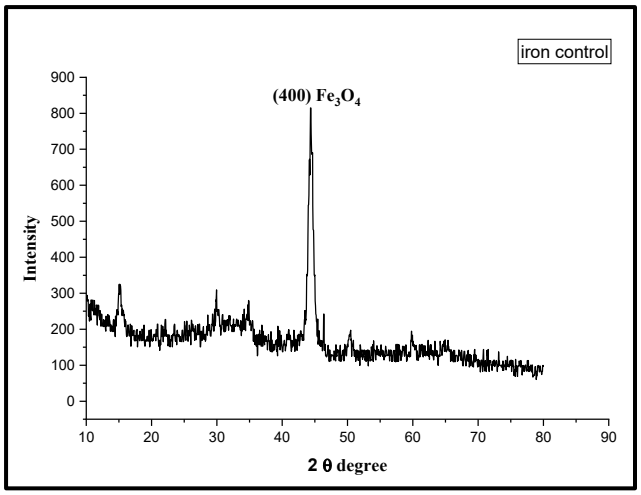

Figure 5. The patterns of XRD analysis of iron oxide before heating and exposure to plasma

According to XRD analysis (Fig. 6), the structural properties of iron oxide films were found to be strongly by exposure to DBD. By providing energy that facilities atomic rearrangement into more order configurations, the plasma drives a transformation from a monocrystalline to a poly-crystalline phases[34], and formation a mixture phases Fe3O4, γ-Fe2O3, and β-Fe2O3 in different orientation. The impact of plasma treatment duration was examining at 2.5, 5, 10, and 15 min. The shortest exposure (2.5 min) produced the highest intensity, while longer exposure time clearly reduced it, indicating lower crystallinity. furthermore, the 15 min treatment caused a phase transformation toward a different orientation.

Probably longer treatment times can increase the energy available for phase transitions, leading to the appearance of new XRD peaks corresponding to different iron oxide phases and the presence of reactive oxygen species that can interact with iron oxide films, leading to phase transformations. For instance, the presence of reactive oxygen species can promote the conversion of maghemite (γ-Fe_2O_3) to other iron oxide phases such as hematite (α-Fe_2O_3). Also Higher oxygen concentrations can lead to the formation of phases with higher oxidation states, such as ε-Fe_2O_3, while lower concentrations favor the formation of magnetite[35,36]. In comparison XRD patterns of iron oxide that annealed by heat, it can be observed in (Fig.7) that there are other peaks are formed which don't exist in the XRD patterns of prepared iron oxide by electrochemical deposition (Fig.5), with reduced intensity than that of the samples that treated with plasma. So, the heating to 200℃ or 400℃ is not adequate for crystallization process or phase stability. taking into account that iron oxide is typically poly crystalline structure and unstable by nature, this causes its properties to change[37,38] In contrast, exposure to plasma led to crystallization, with two phases remaining dominant.

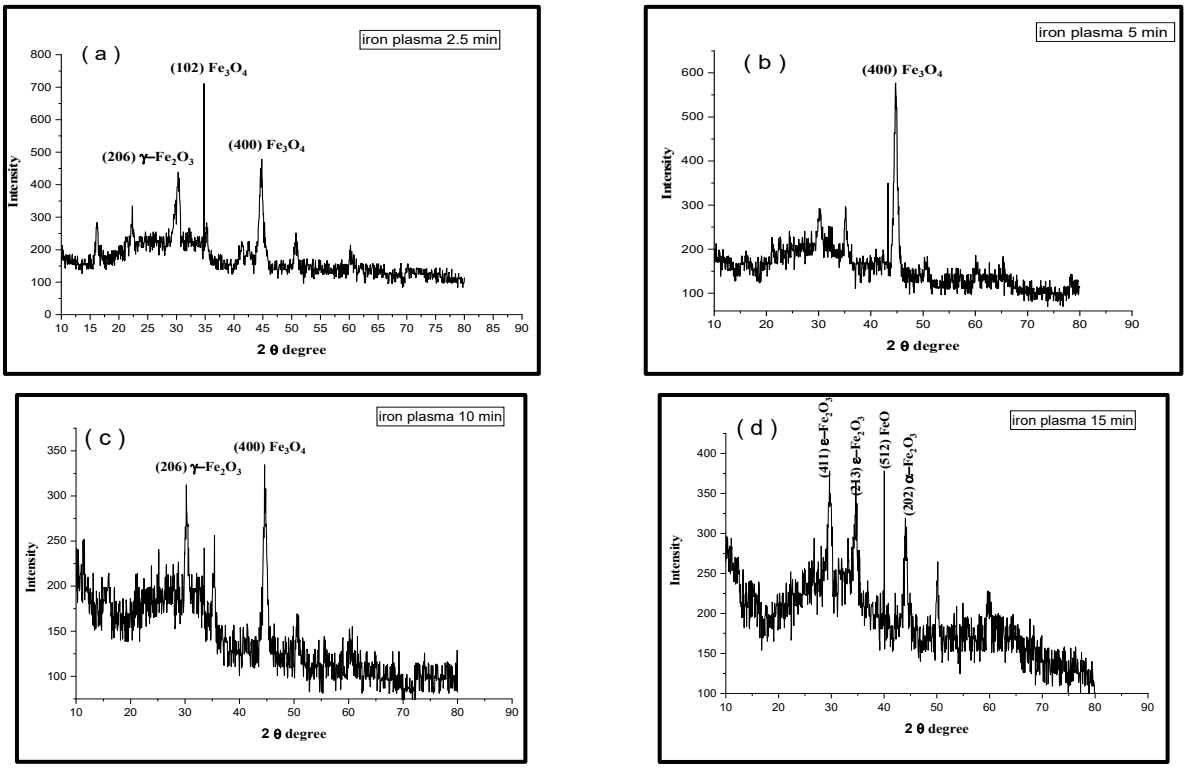

Figure 6. XRD analysis of iron oxide after exposure to plasma for: (a) 2.5 min, (b) 5 min, (c) 10 min, (d) 15 min

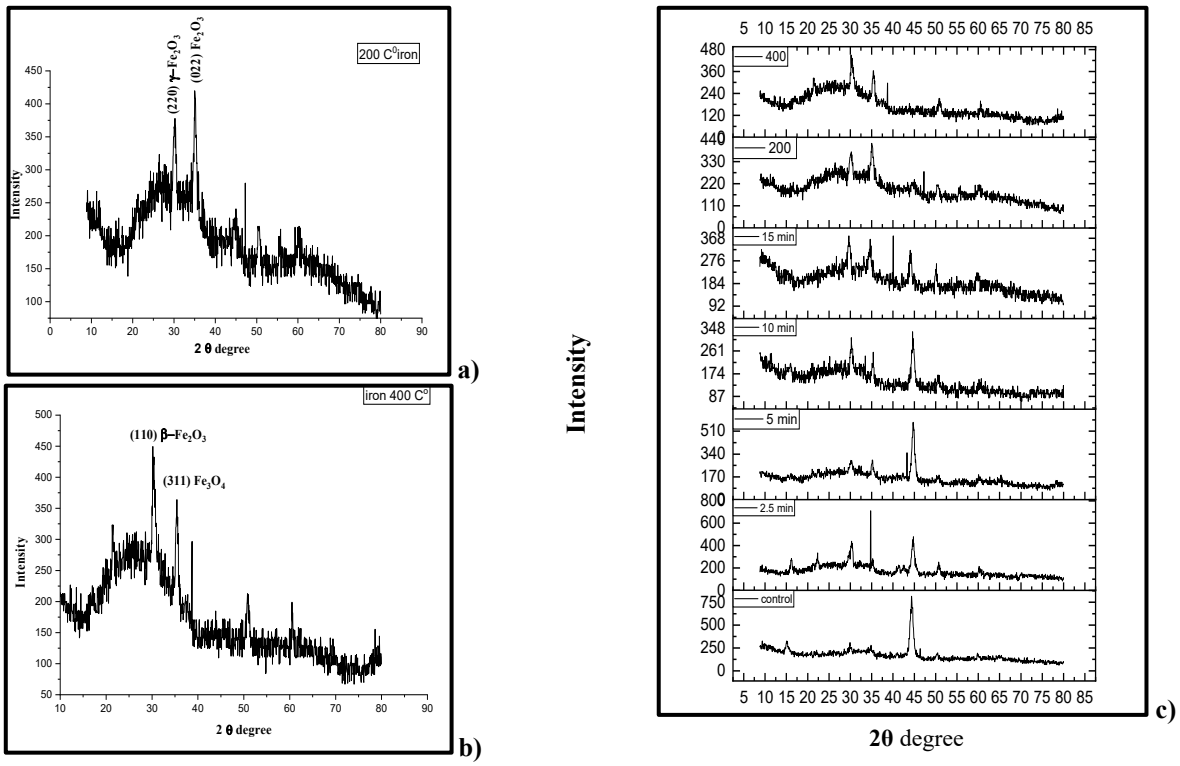

Figure 7. XRD analysis of iron oxide after heating to: (a) 200°C, (b) 400°C,
(c) all treatments (control, (2.5, 5, 10, 15) min, (200, 400)°C

Atomic Force Microscopy (AFM) Analysis of Iron Oxide

The AFM test of prepared iron oxide by electrochemical deposition represented by Fig. (8). the control sample (9 a) showed all values are large of (mean average diameter (≈509 nm), roughness, root mean square (Ra≈133 nm, RMS ≈ 159 nm), and threshold value is (≈244 nm), this indicates that very irregular surface and large sized grains as listed in Table (2).

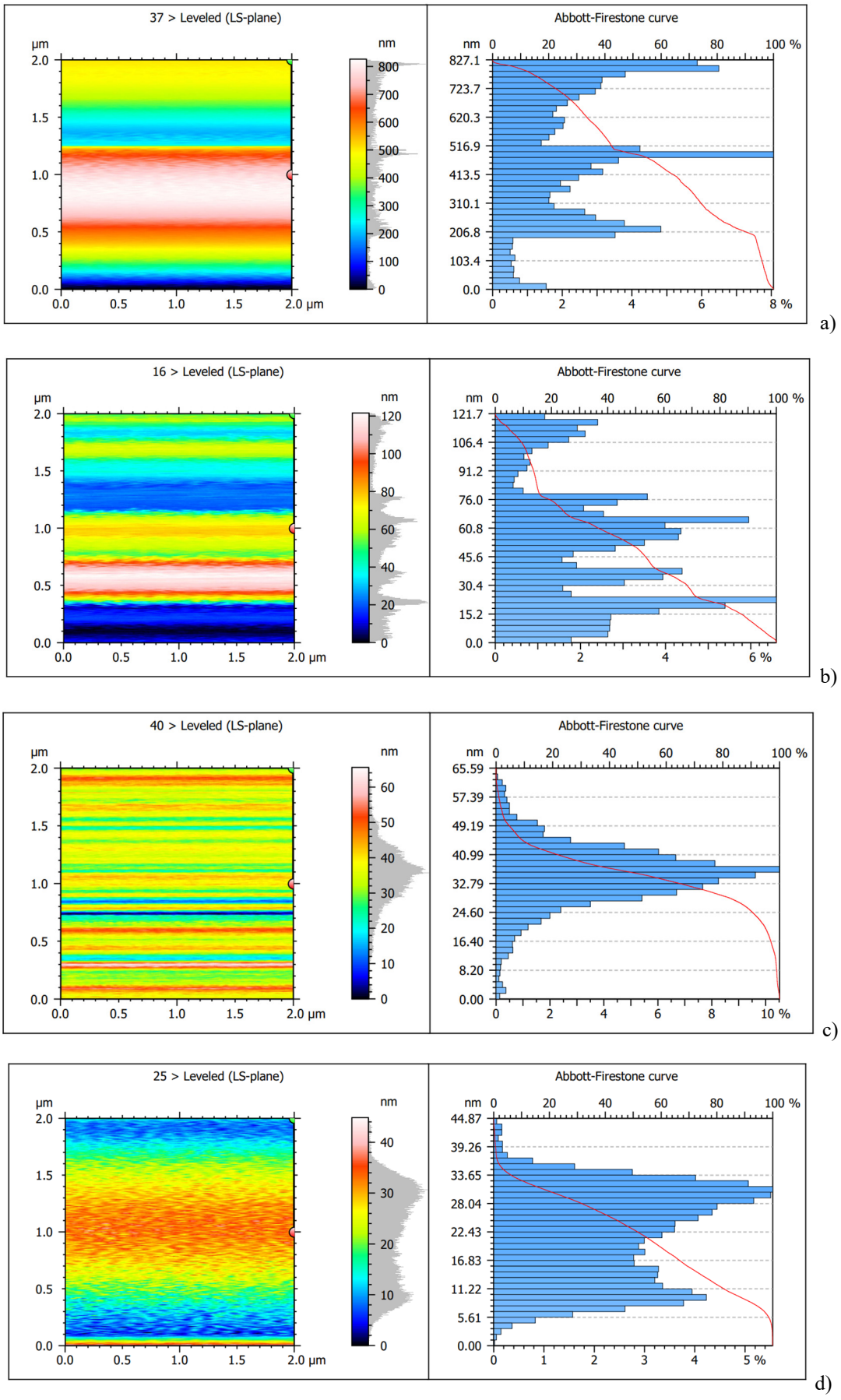

Figure 8. AFM of Iron oxide thin film for: (a) control (b): 2.5 min, (c): 5 min, (d):10 min, (e): 15 min (f) 200°C, (g) 400°C

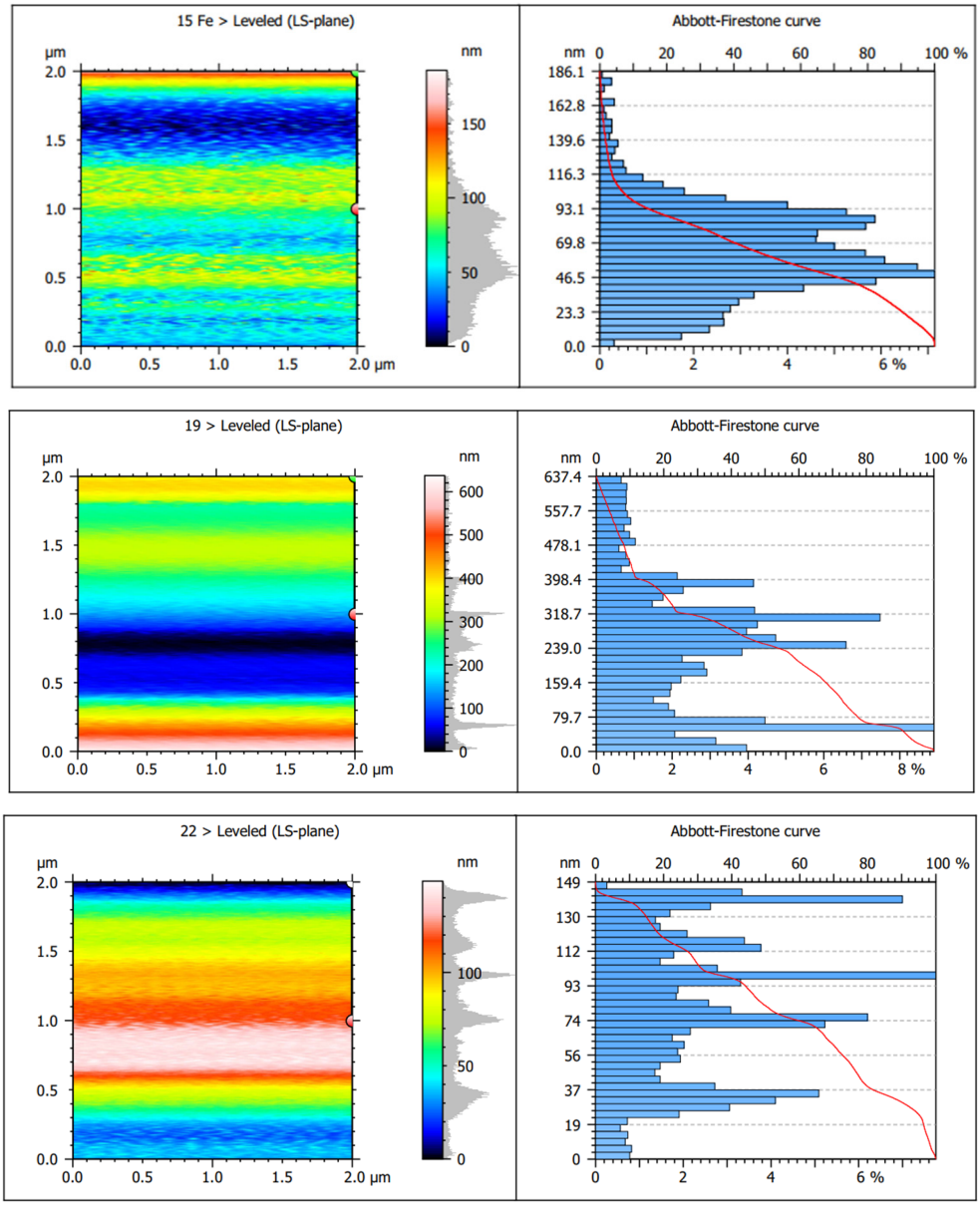

e)

f)

g)

Figure 8. AFM of Iron oxide thin film for: (a) control (b): 2.5 min, (c): 5 min ,(d):10 min, (e): 15 min (f) 200℃, (g) 400℃ (*continued*)

After exposure to cold plasma, we show that at exposure times (2.5, 5, 10 min) gave better results, as shown in Fig. (8 b, c, and d), the grain size decreases and a reduction in roughness and root mean square, as listed in Table (2). This is due to the interaction between the components of cold plasma (ions, free radicals ROS and RNS, UV photons) with surface, plasma etches large grains and rough protrusions at the atomic level, resulting in significant and fast smoothing at a few minutes. When plasma processing time was increased to 15 minutes, as shown in Fig. (8 e), instead of continuing to smooth the surface, the plasma begins to create damage, such as microscopic porous pits or the random redeposition of removed material, which increases the roughness again, this mean arrived at over-treatment or excessive processing. This highlights the importance of precise control over the processing time.

Table 2. Summarized the AFM analysis of iron oxide samples

Samples	Mean diameter (nm)	Surface Roughness (nm)	Root Mean Square (nm)	Threshold(nm)
control	509.2	133.5	159.2	492.8
2.5 min	56.42	21.59	26.20	50.91
5 min	37.62	6.254	8.329	35.13
10 min	23.83	4.763	5.969	21.75
15 min	72.39	22.55	28.65	63.43
200 ºC	292.9	81.82	103.2	241.8
400 ºC	86.67	17.15	22.27	82.62

As a result of annealing that shown in (Fig. 8f) & (Fig.8g), at 200°C the grains remain large (~293 nm) and the surface is rough. The thermal energy is insufficient for true atomic diffusion. It closely resembles the control sample. At 400°C a significant improvement compared to the 200°C sample. The average diameter decreased to ~87 nm, and the surface smoothness improved. The high temperature facilitates recrystallization, where small grains either merge or reorganize into larger, more regular grains, which enhances the overall properties, though not as effectively as the optimal treatment (5 minutes).

CONCLUSIONS

From the above results, the DBD plasma can be an alternative way for annealing for a short time, a few minutes for CAP, in contrast, several hours for annealing. Nickel and iron oxide that deposited by electrochemical deposition, the reactive species in plasma enhanced the interaction and lead to better crystallinity and stability by creating nanoparticles with a flat morphology. So, the plasma achieved the same effect in increasing crystallinity and formation new phases for few minutes comparing with treatment by heat at 200°C and 400°C which needed many hours (according to X-ray diffraction). Also, another conclusion from the results is that the best time was 2.5 minutes, Prolonged plasma exposure introduces energetic ions and reactive species that can etch the film surface create defects, and break down crystalline domains, leading to increased amorphization and reduced crystallinity. AFM results of nickel clarified that the high energy species in plasma DBD bombard the surface and allowed to fill in valleys leading to smoother surface in the time from (2.5 to 10 min), while surface roughness in iron oxide the early stage of plasma exposure increased it leading to etching and the formation of microstructures that increase surface roughness where the presence of atomic hydrogen enhances the reduction of iron oxides, leading to surface modifications, the process reversed with increasing the time, So the AFM results confirmed that the effect of plasma treatment has been changed with time of exposure. And behaved different manner in nickel and iron oxide.

Acknowledgments

We would like to acknowledge the Plasma Physics Laboratory at the Physics Department, College of Science for Women, University of Baghdad, for facilitating this research.

Funding. The authors declare that no funds, grants, or other support were received during the preparation of this manuscript.

Conflict of interest: The authors declare no competing interests.

Data Availability. The experimental datasets generated and analyzed during the current study are openly available in the Zenodo repository at the following permanent "DOI 10.5281/zenodo.17440638, DOI 10.5281/zenodo.17440560, DOI 10.5281/zenodo.17440742, DOI 10.5281/zenodo.17440466."

Author Declaration: This manuscript was written entirely by humans without the use of AI tools. Only Google Translate was used for language translation assistance.

ORCID

Aya Jumaa, https://orcid.org/0009-0008-4601-9686; **Duha K. Harfesh,** https://orcid.org/0000-0003-0950-7804;
A.N. Yasoob, https://orcid.org/0000-0002-0148-5500

REFERENCES

[1] M. Gavahian, and P.J. Cullen, "Cold Plasma as an Emerging Technique for Mycotoxin-Free Food: Efficacy," Mechanisms, and Trends. Food Reviews International, **36**, 193–214 (2019). https://doi.org/10.1080/87559129.2019.1630638

[1] N. Yasoob, K. Khaleel, and H. Murbat, "Study of the Effect of Cold Plasma on the Reproductive Endocrinology of Male Rats," Plant archives, **20**, 526–531 (2020).

[2] G.A. ul J. A. ul Sattar, A.N. Yasoob, "Synthesis and Characterization of Silicon Nanoparticles by Argon Plasma Jet Technique and Its Antibacterial S. Aureus Activity," BioNanoScience, **15**, 202 (2025). https://doi.org/10.1007/s12668-025-01806-9

[3] Y. Shi, Q. Shu, P.K. Liaw, *et al*., "Effect of annealing on mechanical and thermoelectric properties of a Al2CoCrFeNi high-entropy alloy," Materials & design, **213**, 110313–110313 (2022). https://doi.org/10.1016/j.matdes.2021.110313

[4] A.B. El-Bediwi, E. Kashita, and S.M.M. Salman, "Influence of Annealing on Creep Indentation, Surface Properties and Electrochemical Corrosion Behavior of Ni-Cr Based Dental Alloy," International Journal of Applied Sciences and Biotechnology **5**, 366–374 (2017). https://doi.org/10.3126/ijasbt.v5i3.18295

[5] M. Pita, and L. Lebea, "Effect of Annealing on the Microstructure, Hardness, Electrical Conductivity, and Corrosion of Copper Material before Accumulative Roll Bonding Processes," Journal of Engineering, **2022**, 1–8 (2022). https://doi.org/10.1155/2022/6963417

[6] J. Butt, H. Afsharnia, A.Alam, and V. Mohaghegh, "Effect of Different Annealing Methods on ULTEM 9085 Parts Manufactured by Material Extrusion," Journal of Manufacturing and Materials Processing, **8**, 258–258 (2024). https://doi.org/10.3390/jmmp8060258

[7] G.M. Alonzo-Medina, A. González-González, J.L. Sacedón, and A.I. Oliva, "Understanding the thermal annealing process on metallic thin films," IOP Conference Series: Materials Science and Engineering, **45**, 012013 (2013). https://doi.org/10.1088/1757-899x/45/1/012013

[8] R. Wang, Z. Xia, X. Kong, et al., "Etching and annealing treatment to improve the plasma-deposited SiOx film adhesion force," Surface and Coatings Technology, **427**, 127840 (2021). https://doi.org/10.1016/j.surfcoat.2021.127840

[9] N. Shota, T. Tsutsumi, I. Sakata, and M. Hori, "Plasma processing and annealing for defect management at SiO2/Si interface," Journal of Vacuum Science & Technology B Nanotechnology and Microelectronics Materials Processing Measurement and Phenomena, **41**, (2023). https://doi.org/10.1116/6.0002822

[10] W. Kaczorowski, W. Szymanski, D. Batory, and P. Niedzielski, "Effect of plasma treatment on the surface properties of polydimethylsiloxane," Journal of Applied Polymer Science, **132**, (2014). https://doi.org/10.1002/app.41635
[11] O.V. Byrka, S.S. Herashchenko, V.A. Makhlai, *et al*., "Modification and Alloying Effects In Eurofer Steel Under Powerful Pulsed Plasma Impacts," Problems of Atomic Science and Technology, 191–194 (2021). https://doi.org/10.46813/2021-134-191
[12] Y. Xu, Y. Zhang, T. He, et al., "The Effects of Thermal and Atmospheric Pressure Radio Frequency Plasma Annealing in the Crystallization of TiO2 Thin Films," Coatings, **9**, 357–357 (2019). https://doi.org/10.3390/coatings9060357
[13] O. Kylián, "Atmospheric Pressure Plasma Treatment of Materials," in: *Meeting abstracts/Meeting abstracts (Electrochemical Society CD-ROM) MA2022-02*, (2022), pp.886–886. https://doi.org/10.1149/ma2022-0219886mtgabs
[14] N.A. Yasoob, "Verification and Demonstration of the Ability of Plasma Generated from Dielectric Barrier Discharge to Oxidize," Baghdad Science Journal, **22**, 1295-1303 (2024). https://doi.org/10.21123/bsj.2024.11217
[15] R. Pernica, M. Klíma, P. Londák, and P. Fiala, "Modification of Insulating Properties of Surfaces of Dielectric High-Voltage Devices Using Plasma," Applied Sciences, **14**, 4399 (2024). https://doi.org/10.3390/app14114399
[16] T. Vopát, Š. Podhorský, M. Kuruc, et al.," Advanced approach of forming cutting edge radii on cemented carbide cutting tools using plasma discharges in electrolyte," Journal of Manufacturing Processes, **120**, 778–794 (2024). https://doi.org/10.1016/j.jmapro.2024.04.028
[17] D. Ries, E. Robert, S. Dozias, et al., "Characterisation of plasma sources for biomedical applications," International Plasma Chemistry Society, 5–8 (2011).
[18] S.K. Sharma, and A. Sharma, "Sterilization of Microorganisms Contaminated Surfaces and its Treatment with Dielectric Barrier Discharge Plasma," Transactions of the Indian National Academy of Engineering, **5**, 1 (2020). https://doi.org/10.1007/s41403-020-00124-8
[19] X. Sun, B. Zang, and B. Sun, "Surface Modification of Polyethylene in Dielectric Barrier Discharge (DBD) Plasma under Atmospheric-Pressure," IJEIR, **5**, 164–167 (2016).
[20] O. Polonskyi, T. Hartig, J.R. Uzarski, and M.J. Gordon, "Precise localization of DBD plasma streamers using topographically patterned insulators for maskless structural and chemical modification of surfaces," Applied Physics Letters, **119**, 211601 (2021). https://doi.org/10.1063/5.0071460
[21] W. Zhang, X. Xu, F. Wei, et al., "Influence of Dielectric Barrier Discharge Treatment on Surface Structure of Polyoxymethylene Fiber and Interfacial Interaction with Cement," Materials, **11**, 1873 (2018). https://doi.org/10.3390/ma11101873
[22] C. Sawangrat, P. Thipchai, K. Kaewapai, et al., "Surface Modification and Mechanical Properties Improvement of Bamboo Fibers Using Dielectric Barrier Discharge Plasma Treatment," Polymers, **15**, 1711 (2023). https://doi.org/10.3390/polym15071711
[23] R.W. Cairns, and E. Ott, "X-Ray Studies of the System Nickel—Oxygen—Water. I. Nickelous Oxide and Hydroxide," Journal of the American Chemical Society, **55**, 527–533 (1933). https://doi.org/10.1021/ja01329a013
[24] A. Jumaa, W. Aziz, and M. Abid, "Effect of molar concentration of iron(III) chloride on activity of prepared iron oxide nano-particles for degradation methylene blue," in: *2nd International Conference For Engineering Sciences And Information Technology (Esit 2022)*, (ESIT2022 Conference Proceedings, (2024).
[25] S.H. Choi, J. Kim, and Y.S. Yoon, "Effect of plasma immersion on crystallinity of V_2O_5 film grown by dc reactive sputtering at room temperature," Thin Solid Films, **493**, 1–5 (2005). https://doi.org/10.1016/j.tsf.2004.07.057
[26] M. Jenko, M. Godec, A. Kocijan, et al., "A new route to biocompatible Nitinol based on a rapid treatment with H2/O2 gaseous plasma," Applied Surface Science, **473**, 976–984 (2018). https://doi.org/10.1016/j.apsusc.2018.12.140
[27] F. Hajakbari, S. Rashvand, and A. Hojabri, "Effect of plasma oxidation parameters on physical properties of nanocrystalline nickel oxide thin films grown by two-step method: DC sputtering and plasma oxidation," Journal of theoretical and applied physics, **13**, 365–373 (2019). https://doi.org/10.1007/s40094-019-00350-8
[28] N. Ahmed, W. Luo, R. Zhao, et al., "Role of Plasma in Catalyst Preparation and Modification for Oxygen Evolution Reaction," Precision Chemistry, **3**, (2024). https://doi.org/10.1021/prechem.4c00075
[29] P. Chytrosz-Wrobel, M. Golda-Cepa, E. Stodolak-Zych, et al., "Effect of oxygen plasma-treatment on surface functional groups, wettability, and nanotopography features of medically relevant polymers with various crystallinities," Applied surface science advances, **18**, 100497–100497 (2023). https://doi.org/10.1016/j.apsadv.2023.100497
[30] H. Abdel-Khalek, M.I. El-Samahi, and A.M. El-Mahalawy, "Plasma impact on structural, morphological and optical properties of copper acetylacetonate thin films," Spectrochimica Acta Part A: Molecular and Biomolecular Spectroscopy, **199**, 356–366 (2018). https://doi.org/10.1016/j.saa.2018.04.001
[31] L. Vivet, R. Benoit, M.F. Falzon, et al., "XPS, ToF SIMS and wettability analyses on Ni surfaces after Ar-H2 RF plasma treatment: An efficient and optimized plasma treatment approach," Surface & Coatings Technology, **398**, 126094–126094 (2020). https://doi.org/10.1016/j.surfcoat.2020.126094
[32] M. Quaas, O. Ivanova, C.A. Helm, and H. Wulff, "Influence of reactive plasmas on thin nickel films," Oldenbourg Wissenschaftsverlag eBooks, **27**, 295–302 (2008). https://doi.org/10.1524/9783486992564-036
[33] K.N. Pandiyaraj, M. Karuppusamy, P. Jayamurugan, et al., "Iron oxide nanoparticles (IONPs) synthesized via a novel non-thermal atmospheric pressure plasma-assisted electrolysis: Physicochemical characterization and cytocompatibility evaluation," Advanced Powder Technology, **35**, 104441 (2024). https://doi.org/10.1016/j.apt.2024.104441
[34] M. Serhan, D. Jackemeyer, M. Long, et al., "Total Iron Measurement in Human Serum With a Novel Smartphone-Based Assay," IEEE Journal of Translational Engineering in Health and Medicine, **8**, 1–9 (2020). https://doi.org/10.1109/jtehm.2020.3005308
[35] V. Stranak, Z. Hubicka, M. Cada, et al., "Influence of reactive oxygen species during deposition of iron oxide films by high power impulse magnetron sputtering," Journal of physics D, Applied physics, **51**, 095205–095205 (2018). https://doi.org/10.1088/1361-6463/aaa9e6
[36] W.J. Aziz, Aya Jumaa, and M.A. Abid, "Effect of variation biomass on the properties of iron oxide NPs for hydrolysis of methylene blue dye," Journal of Physics Conference Series, **2322**, 012086–012086 (2022). https://doi.org/10.1088/1742-6596/2322/1/012086

[37] M. Chabane, C. Melkaoui, N. Ferrah, et al., "Synthesis and Evaluation of Polyacrylamide Based Filter Pellets Incorporating GAC, Iron Oxide, Zinc Oxide, and Kaolin for Chromium and Nickel Water Remediation," Revue des composites et des matériaux avancés, **34**, 221–232 (2024). https://doi.org/10.18280/rcma.340212

ПОРІВНЯЛЬНИЙ ВПЛИВ ХОЛОДНОЇ ПЛАЗМИ ТА ТЕРМІЧНОГО ВІДПАЛУ НА СТРУКТУРНІ ТА МОРФОЛОГІЧНІ ВЛАСТИВОСТІ ПОКРИТТІВ З НІКЕЛЮ ТА ОКСИДУ ЗАЛІЗА

Ая Джумаа, Духа К. Харфеш, А.Н. Ясуб, Хамід Х. Мурбат

Багдадський університет, Коледж наук для жінок, кафедра фізики, Багдад, Ірак

У цьому дослідженні всебічно досліджується та порівнюється вплив обробки холодною атмосферною плазмою (ХАТП) як потенційної альтернативи термічному відпалу на структурні та морфологічні властивості двох різних тонких плівок: нікелю (Ni) та оксиду заліза (Fe_xO_y), обидві електрохімічно нанесені на підкладки ITO. Характеристика за допомогою рентгенівської дифракції (XRD) та атомно-силової мікроскопії (АСМ) показала, що природа матеріалу визначає його реакцію на постобробку. Для нікелю короткочасна обробка CAP (2,5-5 хв) оптимально покращувала кристалічність та гладкість поверхні за рахунок зменшення розміру зерен та шорсткості, тоді як триваліша обробка призводила до окислення та збільшення шорсткості. І навпаки, для оксиду заліза навіть короткочасна обробка CAP ініціювала перехід від монокристалічної до полікристалічної структури, утворюючи суміш фаз (Fe_3O_4, γ-Fe_2O_3). Найгладша поверхня оксиду заліза була досягнута після 5-10 хвилин CAP, а надмірна обробка (15 хв) спричиняла пошкодження поверхні. Термічний відпал виявився кращим для нікелю при 200°C, даючи найдрібніші зерна та найгладшу поверхню. Однак цього було недостатньо для оптимальної кристалізації оксиду заліза. Ця робота демонструє, що CAP є швидкою та енергоефективною альтернативою традиційному відпалу. Оптимальні параметри сильно залежать від специфіки матеріалу та мають вирішальне значення для створення функціональних покриттів у каталізі та сенсориці.

Ключові слова: *холодна плазма; DBD; плазмовий відпал; нікелеве покриття; оксид заліза; гематит; магнетит*